

Viscous friction acting on a solid disk falling in confined fluid: Lessons for the scaling analysisNana Tanaka and Ko Okumura ^{*}*Physics Department and Soft Matter Center, Ochanomizu University, 2-1-1 Ohtsuka, Bunkyo-ku, Tokyo 112-8610, Japan*

(Received 19 December 2022; accepted 17 August 2023; published 29 September 2023)

We fill a viscous liquid in a vertically stood cell of millimeter thickness, called the Hele-Shaw cell, and insert a disk in the liquid whose thickness is smaller than the cell thickness. The disk starts falling in the liquid due to gravity opposed by viscous friction. We focus on the case in which lubricating films formed in the gap between the cell surface and the disk surface are thinner than the disk thickness. As a result, we find an apparent scaling regime for the falling velocity of a disk, in which the thickness of the lubricating film characterizes the dynamics. We further show that the apparent scaling regime is explained simply as a result of competition of two scaling regimes, elucidating the physics of the viscous friction. The present study is thus relevant to fundamental issues and applications in various fields in which small-scale physics in the flow at low Reynolds numbers is essential, such as microfluidics, bioconvection, and active matter. The simple scenario for explaining an apparent scaling law demonstrated in the present study would be useful in diverse fields, considering that the generality and strength of scaling analysis in science and that simple arguments usually lead to a few different scaling laws for a given problem.

DOI: [10.1103/PhysRevResearch.5.L032047](https://doi.org/10.1103/PhysRevResearch.5.L032047)

Scaling analysis has been a powerful tool in various fields in science beyond physics [1,2] and applied mathematics [3], which include biology [4,5], engineering [6], and astronomy [7]. A lot of scaling laws have been established with a well-defined scaling exponent, with successful explanations by renormalization group [1,2] or a simple scaling argument. However, it also happens frequently that, although an exponent is clearly observed, a simple argument predicts an exponent slightly deviating from the observed one, as in, for example, the metabolic-rate (R) vs body-mass (M) relation in biology [8] and the luminosity (L) vs mass (M) relation in astronomy [9]: For the relation $R \simeq M^\alpha$ ($L \simeq M^\beta$), experimental data clearly give $\alpha \approx 3/4$ ($\beta \approx 3.7$), while a simple dimensional analysis predicts $\alpha = 2/3$ ($\beta = 3$). Such apparent scaling laws have been interpreted in case-specific or ad hoc theories, leaving room for debate. Here, we focus on a simple viscous dynamics and demonstrate an apparent scaling law, which is simply explained as a result of competition of two scaling regimes. This simple scenario would be useful for understanding apparent scaling laws in diverse fields in science, if one notes that simple scaling arguments usually result in a few different scaling regimes for a given problem.

In addition to the significance in the general context of the scaling analysis, the present study could be fundamentally important for various current topics such as microfluidics [10], promising for applications in chemistry, biology, medicine,

and the pharmaceutical industry, and bioconvection [11–13], which is created via swimming of a large number of small objects and has received attention in active matter and biology. The central issue is the flow at low Reynolds numbers governed by viscous friction due to small scales at which most liquids, including water, are highly viscous.

Relevant classic studies on viscous friction are motion of a bubble in a capillary tube [14] and in a Hele-Shaw cell [15]. Our focus is on the latter. A number of studies have been performed in the Hele-Shaw geometry, with a main focus on a forced flow and/or with nearly horizontal geometries [16–19]. Recently, we have highlighted the existence of lubricating film between the cell surface and bubble surface using a vertically stood Hele-Shaw cell of millimeter thickness filled with viscous liquid to confirm a number of scaling regimes for drag friction acting on fluids surrounded by another immiscible fluid [20–23]. Other groups have explored closely related issues, using cells with smaller scales [24,25] and comparing numerical results with experiments [26].

In this study, we explore a seemingly simpler case of drag friction acting on a solid disk in a Hele-Shaw cell of millimeter thickness, where similar lubricating films exist between the cell wall and disk surface. Our principal interest is in the case in which the thickness of the lubrication film is smaller than the disk thickness when the disk is falling in the direction perpendicular to its axis. As far as we know, this case has not been explored in the literature, while it is closely related to a study of transport of strongly confined disks under flow in microfluidic devices [27]. As a result, we identified an apparent scaling regime, in which the observed scaling exponent for collapsed data deviates from a predicted exponent. We reveal that the deviation is simply the result of competition of two scaling regimes.

In experiments, we filled a Hele-Shaw cell, stood vertically, with a silicone oil (polydimethylsiloxane, PDMS) as shown

^{*}Corresponding author: okumura@phys.ocha.ac.jp

Published by the American Physical Society under the terms of the [Creative Commons Attribution 4.0 International](https://creativecommons.org/licenses/by/4.0/) license. Further distribution of this work must maintain attribution to the author(s) and the published article's title, journal citation, and DOI.

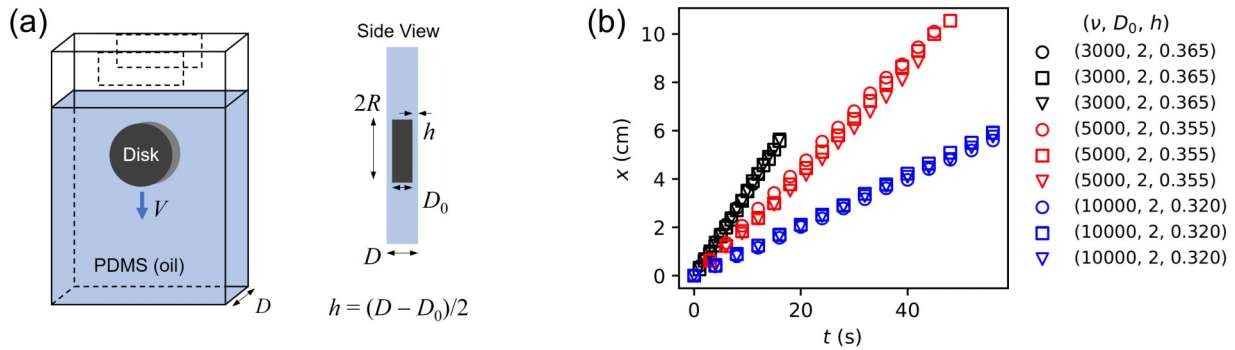


FIG. 1. (a) Illustration of experiment. A metal disk of thickness D_0 is dropped in the cell of thickness D filled with a viscous oil of kinematic viscosity ν . The side view suggests the existence of two lubricating films of thickness h . The two dashed rectangles at the top of the cell on the left indicate the places at which plates (of thickness $\simeq h$) are set (see text for details). (b) Vertical position x vs time t . Results of three falling experiments are shown for each parameter set specified by (ν, D_0, h) . ν is given in centistokes (cS), while D_0 and h are given in millimeters (mm). (See the text for the precise value of D_0 .)

in Fig. 1(a). We inserted a metal disk of radius $R = 10$ mm at the top of the cell with a zero initial speed. We recorded the ensuing falling motion of the metal with a camera after the disk began going down in the cell at a constant speed. The width and height of the cell was 90 and 160 mm, respectively. We checked the thickness D of the cell using a laser sensor (ZS-HLDS5, Omron) and its controller (ZS-HLDC11, Omron) to find D was in the range of 2.2–7 mm (except for a dataset shown by the square in Fig. 2 below). The kinematic viscosity ν of PDMS was in the range of 1000–10000 cS, which corresponds to the range of the viscosity $\eta = \rho_0\nu$, 0.970–9.75 Pa s (the density ρ_0 was in the range 970–975 kg/m³). The metal disk was a stainless-steel SUS403 of density $\rho = 7.70$ g/cm³, which could be manipulated by a magnet placed on the cell surface. The thickness D_0 ($< D$) of the disk was either 1.88, 2.87, or 3.90 mm (these three thicknesses will be labeled as $D_0 = 2, 3,$ and 4 mm, for convenience, in Figs. 1–3). We used a digital camera (EX-F1, Casio), setting the time interval in the range of 1 to 1/60 s. The digital images were analyzed with software IMAGE J.

As demonstrated in Fig. 1(b), the velocity of falling motion of the disk reached a constant speed, which was reproducible at a given experimental parameter set, $\eta, D_0,$ and h (an error in velocity is typically less than 10%). Here, h is the thickness of two viscous liquid films, each of which is sandwiched by the inner surface of cell plate and the surface of the disk.

Obtaining reproducible data as in Fig. 1(b) is highly non-trivial. The main difficulty is to drop the disk in the cell while precisely maintaining the relation $2h = D - D_0$. The falling speed is expected to be maximized when this relation is satisfied with no tilting. Thus, we created a gate by setting two plates of thickness slightly larger than h at the places indicated by the two dashed rectangles at the top of the cell in Fig. 1(a) to help guarantee the condition at the entry. Even with this gate, we need to carefully insert the disk into the gate and collect the data in fast-falling cases. In this way, we could obtain reproducible data as specified above.

In Fig. 2, we present the falling velocity V , obtained as a slope in the $x - t$ plot as in Fig. 1(b), as a function of the film thickness h for $h < D_0$ [except for the rightmost data set (8 data) shown by the square in Fig. 2(b), for which $h \gtrsim D_0$]. One data point shown without error bars corresponds to each falling experiment. We repeated falling experiments typically several times (in the range of two to more than ten times) for a single parameter set and we showed all the results in the plots. As a result, in some cases data points are closely overlapped, which suggests a small size of errors in the measurements.

The viscosity dependence of the velocity in Fig. 2 indicates that the dynamics is governed by gravity opposed by viscosity. In fact, the inertia can be neglected in most (practically all, as revealed below) of the data. This is because, writing the Reynolds number Re as ρ_0VL/η with introducing a length

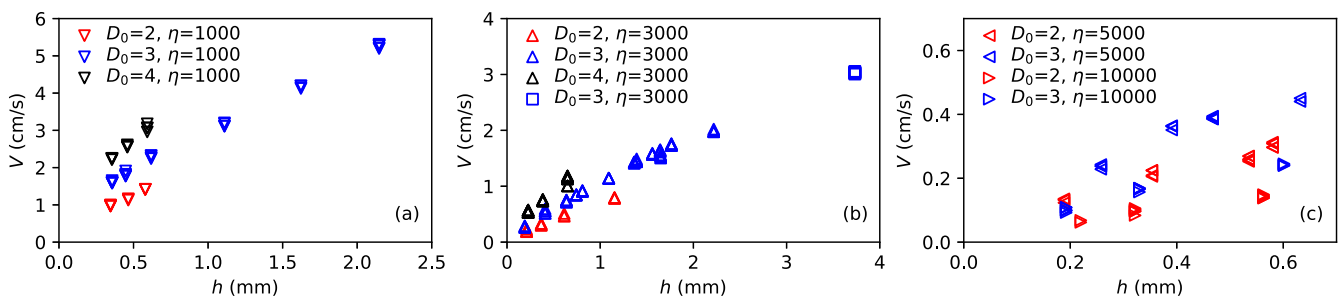


FIG. 2. V vs h for $h < D_0$. (a) $\nu = 1000$ cS. (b) $\nu = 3000$ cS. (c) $\nu = 5000$ and 10000 cS. Colors and marks differentiate D_0 and ν , respectively (the square is an exception). The labels for D_0 and ν are given in mm and cS. The number of the data points shown here are 240 in total and they are obtained for 46 different parameter sets (D_0, η, h) . (The precise values of D_0 are given in the text.)

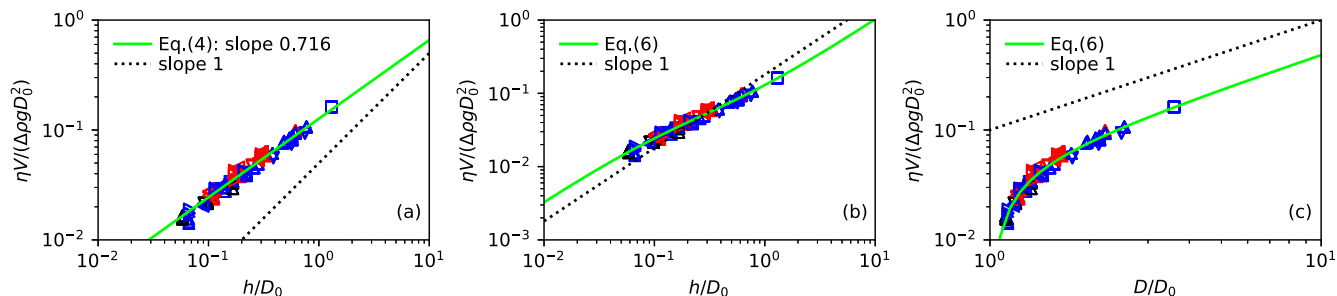


FIG. 3. Renormalized velocity V vs thickness h for the 240 data in Fig. 2. (a) Fit by Eq. (4) with $\alpha = 0.716$. The slope of the fit (solid line) deviates from the slope of the dotted line, which corresponds to $\alpha = 1$. (b) Successful fit by Eq. (6) with the same renormalized axes with (a). (c) The same successful fit by Eq. (6) but with a differently renormalized horizontal axis.

scale L , the condition $\text{Re} < 1$ is equivalent to $L < \eta/(\rho V)$, where the average and minimum of $\eta/(\rho V)$ are 1.5 and 0.02 m, while L in the present case is either h, D_0, D , or R , which are all smaller than even the minimum of $\eta/(\rho V)$.

Theoretically, the change in gravitational energy per time is trivially given as $\pi \Delta \rho g R^2 D_0 V$ with $\Delta \rho = \rho - \rho_0$. As for the viscous dissipation, we can think of three possibilities, corresponding to three viscous length scales, h , D , and R . The first one, $\eta(V/h)^2 R^2 h$, which we call the h dissipation, describes dissipation inside the lubrication film of thickness h with its volume scaling as $R^2 h$. The second D dissipation $\eta(V/D)^2 R^2 D$ is associated with the viscous flow developed between the cell plates separated by the distance D in a volume scaling as $R^2 D$. The third R dissipation $\eta(V/R)^2 R^2 D$ corresponds to the dissipation with the viscous length scale R developed in a volume scaling as $R^2 D$. If we compare the three dissipations with their coefficients set to unity, the ratios of the D and R dissipations to the h dissipation are h/D and hD/R^2 , respectively, both of which are less than unity in the present experiment. More precisely, the average and median of the first ratio h/D are 0.16 and 0.14, while those of the second ratio hD/R^2 are 0.039 and 0.018.

As a first trial for comparison between theory and experiment, we assume the largest h dissipation dominates over the other dissipations. Then, the balance of the change in gravitational energy with dissipation (the h dissipation only) gives

$$V \sim \Delta \rho g D_0 h / \eta, \quad (1)$$

which can be expressed as

$$\eta V / (\Delta \rho g D_0^2) = f(h/D_0) \quad (2)$$

with

$$f(x) \simeq x. \quad (3)$$

In Fig. 3(a), we plot the renormalized velocity $\eta V / (\Delta \rho g D_0^2)$ as a function of the renormalized thickness h/D_0 , in light of Eq. (2), using all the data in Fig. 2, where the data described by Eq. (1) should collapse onto a master curve on this plot. This is what we observe in Fig. 3(a): All the data in Fig. 2 (except the data set with $h \gtrsim D_0$) collapse well on a master curve.

However, the agreement is not perfect. As a result of numerical fitting, we find that the collapsed data are well described by the following expression:

$$\eta V / (\Delta \rho g D_0^2) = k_1 (h/D_0)^\alpha, \quad (4)$$

with $k_1 = 0.127 \pm 0.001$ and $\alpha = 0.716 \pm 0.008$ (in this fitting, the data set with $h \gtrsim D_0$ is excluded). The exponent α deviates from the theoretical prediction $\alpha = 1$.

This deviation cannot be explained by the slip length which has been discussed for polymer liquids [1,28]. This is because a simple linear extrapolation of the data of each color in Fig. 2(a) may intersect the horizontal axis at a value around $h = -0.1$ to -0.3 mm, and this order of magnitude is too large for the slip length (in the present case, it is at most $10 \mu\text{m}$).

As a second trial, we include the second largest D dissipation in addition to the h dissipation, since the first trial based on the h dissipation only raised problems. Then, the new energy balance can be cast in the following form:

$$\Delta \rho g R^2 D_0 V = \eta V^2 R^2 (c_1/h + c_2/D), \quad (5)$$

where c_1 and c_2 are numerical coefficients (the two energy dissipations are added here, considering a simplest and physically plausible case). This leads to Eq. (2) with

$$f(x) = \frac{d_1 x}{1 + \frac{d_2 x}{1+2x}}, \quad (6)$$

where $d_1 = 1/c_1$ and $d_2 = c_2/c_1$.

Equation (6) still predicts a data collapse when $\eta V / (\Delta \rho g D_0^2)$ is plotted as a function of h/D_0 , which is truly observed in Fig. 3(a). In Fig. 3(b), the same plot is presented with the result of an excellent fitting by Eq. (2) with (6), where $d_1 = 0.34 \pm 0.01$ and $d_2 = 4.90 \pm 0.26$. Note that even the data set with $h \gtrsim D_0$ is well fit by Eq. (6), although this set is excluded in the fitting. Since $d_2 = c_2/c_1$ corresponds to the relative importance of the D dissipation to the h dissipation as seen in Eq. (5), the present fitting predicts that the two dissipations are comparable and the D dissipation is larger than the h dissipation.

However, the D dissipation does not play a dominant role. This is clearly shown in Fig. 3(c). To understand this, note that Eq. (2) with Eq. (6) can be expressed as

$$\eta V / (\Delta \rho g D_0^2) = (1/c_2)(D/D_0) \quad (7)$$

when the D dissipation dominates over the h dissipation, i.e., if $c_1 \ll c_2$. This means if the D dissipation is dominant we should observe that most of the collapsed data are on a line with slope 1 in Fig. 3(c), which is not the case. We emphasize here that the data set with $h \gtrsim D_0$ (square) in Fig. 3(c) significantly strengthens our arguments for the D dissipation,

supporting the approach to a line with slope 1 as D/D_0 increases. Note that thanks to the relation $D/D_0 = 1 + 2h/D_0$ when the plot $\eta V/(\Delta\rho g D_0^2)$ vs h/D_0 collapses onto a master curve as in Fig. 3(b), so does the plot $\eta V/(\Delta\rho g D_0^2)$ vs D/D_0 as in Fig. 3(c).

Further insight can be obtained if we note the following limiting forms for Eq. (6):

$$f(x) = \begin{cases} d_1 x & x \ll 1 \\ [d_1/(1 + d_2/2)]x & x \gg 1. \end{cases} \quad (8)$$

These limiting behaviors can be observed in Fig. 3(b) with the aide of the dotted line with slope 1. In between there exists a quasi-straight-line region with data collapsed. Such a straight-line region, if it exists, should possess a slope smaller than 1, since the first coefficient d_1 is larger than the second coefficient $d_1/(1 + d_2/2)$ in Eq. (8) and, thus, the second slope 1 region ($x \gg 1$) is shifted below the first ($x \ll 1$), as can be confirmed in Fig. 3(b). This is the reason we obtained α less than 1 in the above. Note that the data set with $h \gtrsim D_0$ is consistent with this argument: All the data in Fig. 3(b) fit well in the region between the apparent scaling with slope α and the linear scaling with slope 1 for $x \gg 1$ in Eq. (8), where the set with $h \gtrsim D_0$ is in the region rather close to the starting of the linear scaling. Further note that while the linear scaling for $x \ll 1$ corresponds to the real scaling for the h dissipation, that for $x \gg 1$ might look in consistent with the real scaling for the D dissipation, which, in light of Eq. (7) below, can be expressed as $(1 + 2x)/c_2$. This concern is resolved if one notices the second coefficient $d_1/(1 + d_2/2)$ in Eq. (8) approaches $2/c_2$ in the limit $c_2 \gg c_1$.

For completeness, we explain the reason we can neglect the R dissipation, although this dissipation is expected to be the smallest. We rewrite the balance in Eq. (5), including the R dissipation: $\Delta\rho g R^2 D_0 V = \eta V^2 R^2 (c_1/h + c_2/D + c_3 D/R^2)$, to obtain Eq. (2) with

$$f(x) = \frac{d_1 x}{1 + \frac{d_2 x}{1+2x} + d_3 \left(\frac{D_0}{R}\right)^2 x(1 + 2x)}. \quad (9)$$

This form predicts that, if the d_3 term cannot be neglected, the collapse onto a master curve cannot be observed in Fig. 3 (because the data includes those obtained for different D_0 with R fixed), which is not true. Thus, we can judge that the remaining R dissipation can be safely neglected from our argument to explain the collapsed data.

We can learn two lessons from the present analysis. (1) When a log-log plot is seen in a limited range, in principle, it tends to seem like a straight line, and when the slope is fairly close to the one predicted from a simple dimensional analysis, one tends to overlook other important physical origin of the problem. (2) In such a case, or even when such an apparent scaling regime spans over a few or several decades, when the exponent deviates from the one predicted from a simple argument, it is worth considering competition of a few scaling regimes, as simply demonstrated in the above.

The present apparent scaling regime demonstrated in Fig. 3(a) spans at least over one order of magnitude, but a limited range. According to the theory, our data happen to correspond to the ones in the crossover region between the two asymptotic regimes defined in Eq. (8). Judging from the behavior of Eq. (8) shown in Fig. 3(b), we need to further

explore regions $h/D_0 < 0.01$ and > 1 to completely confirm our argument by explicitly establishing real scaling regimes originating from h and D dissipations (in addition to the apparent scaling regime). This implies that we need to explore over four orders of magnitude for h/D_0 in total, which is an important but experimentally challenging future problem. Note here that the real scaling for the D dissipation is already reasonably well confirmed in Fig. 3(c) as mentioned above with the help of the data set with $h \gtrsim D_0$.

We discuss here a semiquantitative estimate for $c_1 = 1/d_1$, which can be obtained in the following way. The velocity gradient could be precisely V/h (assuming a simple Couette shear flow as in the film between two infinite plates separated by h) almost everywhere on the disk surface except near the edge in the small h limit. Then, in this limit, the total drag force might be obtained simply by multiplying this gradient by the viscosity η and the area of both disk surfaces $2\pi R^2$. Balancing the force thus obtained with the gravitational force $\pi R^2 D_0 \Delta\rho g$, we could obtain a plausible value $d_1 = 1/2$ (this leads to a one-parameter fitting in Fig. 3(b), resulting in $d_2 = 9.25 \pm 0.08$). It is interesting that this plausible value is not far from the previous value ($d_1 = 0.34$). However, the data for small h/D_0 in the present study slightly better support the previous fitting shown in Fig. 3(b). This issue could be another motivation for a separate study for $h/D_0 < 0.01$ and > 1 .

As for the coefficient c_2 , when not a solid disk but a fluid drop (viscosity η') moving in a Hele-Shaw cell filled with another viscous fluid (viscosity η), the formula $V = (1/12)\Delta\rho g D^2/\eta$ is derived in the limit $\eta' = 0$ and $D = D_0$ in Ref. [17] from a result in Ref. [15], which has been confirmed by different methods [29,30]. While the present case corresponds $\eta' \gg \eta$ and $D = D_0 + 2h$, if the formula could be applied, it would predict $c_2 = 12$. This estimate is also not far from the value of c_2 obtained from the two-parameter fitting as well as the one-parameter fitting: In the former case $c_2 = d_2/d_1 = 4.9/0.34$ and in the latter case $c_2 = 9.25/(1/2)$.

The present result can be appreciated in the context of a Stokes drag friction F for a solid disk moving in a direction perpendicular to the axis, i.e., in a direction of the disk plane, in a confined geometry specified by two parameters: A measure of confinement $C = R/D$ and the aspect ratio of the disk $A = D_0/R$. Under no confinement ($C = 0$) for a disk of zero thickness ($A = 0$), the drag friction was given by Oberbeck [31] as $F_0 = 32\eta VR/3$. After the case of $A = 0$ and small C was studied [32,33], the case of $C = 0$ and $A \neq 0$ was considered [34]. Then, the case of $C \neq 0$ and $A \neq 0$ was reported [35], where the case with $h < D_0$ was not studied, which is the main focus of the present study. In terms of the drag friction force $F (= KF_0)$, the present study ($0.05 \lesssim h/D \lesssim 0.3$) predicts the following viscous drag and drag coefficient: $F = \pi\eta VR^2(c_1/h + c_2/D)$ and $K = (3\pi R/32)(c_1/h + c_2/D)$, with c_1 and c_2 given through the above values of d_1 and d_2 . Note that K represents the enhancement of the friction due to confinement and thus becomes significantly larger than one under a strong confinement in which $R \gg h$ and D . This implies that the falling velocity in the present confined case is $(3\pi/4)(D_0/R)/K$ times slower than the nonconfined case.

The present falling disk problem is inherently different from the case in which the disk is replaced with a fluid ‘‘disk.’’ Such a case is studied under no existence of surfactants [21],

in which the thickness of lubricating film h and the disk thickness (or the shape of fluid drop) are dynamically determined and thus dependent on V , with the former governed by the law of Landau, Levich, and Derjaguin (LLD) [36,37]. The drag force F thus found scales with $V^{1/3}$, in contrast to the present case, in which h is fixed by the (fixed) disk thickness and F scales simply with V .

More complex cases with rigid and mobile surfactants are relevant if fluid drops of various kinds, such as armored bubbles or drops, gelified drops, bubbles, and drops with surfactants, are utilized. Such cases have been explored mainly on a smaller-length scale appropriate for microfluidics [38,39]. While direct comparison of such studies with the present case may be irrelevant because of the inherent difference in how the thickness of the lubricating film is determined, the study of cases with surfactants on a larger centimeter scale as in the present study will be an important future problem.

In the present study, we investigated the falling velocity of a solid disk in viscous liquid in a confined space and the drag friction acting on the disk. We identified an apparent scaling regime, in which two scaling regimes cooperate. The present study provides a simple possibility of explaining an apparent scaling law, which would be useful to any physical scientists, considering the generality and strength of scaling analysis in science. In addition, fundamental understandings on fluid flow at low Reynolds numbers provided in the present study could be valid for small objects in less viscous fluid such as water. Accordingly, the present study is relevant to various fundamental issues and applications—for example, in microfluidics, bioconvection, and active matter—in which viscous friction acting on small objects is highly important.

This work was partly supported by JSPS KAKENHI Grant No. JP19H01859.

-
- [1] P.-G. De Gennes and P.-G. Gennes, *Scaling Concepts in Polymer Physics* (Cornell University Press, Ithaca, 1979).
- [2] J. Cardy, *Scaling and Renormalization in Statistical Physics* (Cambridge University Press, Cambridge, 1996).
- [3] G. I. Barenblatt, *Scaling* (Cambridge University Press, Cambridge, 2003), Vol. 34.
- [4] J. T. Bonner and T. A. McMahon, *On Size and Life* (Scientific American Library, New York, 1983).
- [5] K. Schmidt-Nielsen and S.-N. Knut, *Scaling: Why is Animal Size So Important?* (Cambridge University Press, Cambridge, 1984).
- [6] L. J. Gibson, M. F. Ashby, and B. A. Harley, *Cellular Materials in Nature and Medicine* (Cambridge University Press, Cambridge, 2010).
- [7] A. R. Choudhuri, *Astrophysics for Physicists* (Cambridge University Press, Cambridge, 2010).
- [8] M. Kleiber, Body size and metabolism, *Hilgardia* **6**, 315 (1932).
- [9] E. Boehm-Vitense, *Introduction to Stellar Astrophysics. Vol. 1: Basic Stellar Observations and Data* (Cambridge University Press, Cambridge, 1989).
- [10] T. M. Squires and S. R. Quake, Microfluidics: Fluid physics at the nanoliter scale, *Rev. Mod. Phys.* **77**, 977 (2005).
- [11] M. A. Bees, Advances in bioconvection, *Annu. Rev. Fluid Mech.* **52**, 449 (2020).
- [12] A. Kage, C. Hosoya, S. A. Baba, and Y. Mogami, Drastic reorganization of the bioconvection pattern of chlamydomonas: Quantitative analysis of the pattern transition response, *J. Exp. Biol.* **216**, 4557 (2013).
- [13] S. Ramaswamy, The mechanics and statistics of active matter, *Annu. Rev. Condens. Matter Phys.* **1**, 323 (2010).
- [14] F. P. Bretherton, The motion of long bubbles in tubes, *J. Fluid Mech.* **10**, 166 (1961).
- [15] G. Taylor and P. G. Saffman, A note on the motion of bubbles in a Hele-Shaw cell and porous medium, *Q. J. Mechanics Appl. Math.* **12**, 265 (1959).
- [16] S. Tanveer, The effect of surface tension on the shape of a Hele-Shaw cell bubble, *Phys. Fluids* **29**, 3537 (1986).
- [17] T. Maxworthy, Bubble formation, motion and interaction in a Hele-Shaw cell, *J. Fluid Mech.* **173**, 95 (1986).
- [18] A. R. Kopf-Sill and G. M. Homsy, Bubble motion in a Hele-Shaw cell, *Phys. Fluids* **31**, 18 (1988).
- [19] S. R. K. Maruvada and C.-W. Park, Retarded motion of bubbles in Hele-Shaw cells, *Phys. Fluids* **8**, 3229 (1996).
- [20] A. Eri and K. Okumura, Viscous drag friction acting on a fluid drop confined in between two plates confined in between two plates, *Soft Matter* **7**, 5648 (2011).
- [21] M. Yahashi, N. Kimoto, and K. Okumura, Scaling crossover in thin-film drag dynamics of fluid drops in the Hele-Shaw cell, *Sci. Rep.* **6**, 31395 (2016).
- [22] K. Okumura, Viscous dynamics of drops and bubbles in Hele-Shaw cells: Drainage, drag friction, coalescence, and bursting, *Adv. Colloid Interface Sci.* **255**, 64 (2018).
- [23] M. Murano and K. Okumura, Rising bubble in a cell with a high aspect ratio cross-section filled with a viscous fluid and its connection to viscous fingering, *Phys. Rev. Res.* **2**, 013188 (2020).
- [24] L. Keiser, K. Jaafar, J. Bico, and É. Reyssat, Dynamics of non-wetting drops confined in a Hele-Shaw cell, *J. Fluid Mech.* **845**, 245 (2018).
- [25] L. Keiser, A. Keiser, M. Lestimé, J. Bico, and E. Reyssat, Motion of Viscous Droplets in Rough Confinement: Paradoxical Lubrication, *Phys. Rev. Lett.* **122**, 074501 (2019).
- [26] I. Shukla, N. Kofman, G. Balestra, L. Zhu, and F. Gallaire, Film thickness distribution in gravity-driven pancake-shaped droplets rising in a Hele-Shaw cell, *J. Fluid Mech.* **874**, 1021 (2019).
- [27] W. E. Uspal, H. B. Eral, and P. S. Doyle, Engineering particle trajectories in microfluidic flows using particle shape, *Nat. Commun.* **4**, 2666 (2013).
- [28] P. G. de Gennes, *Soft Interfaces: The 1994 Dirac Memorial Lecture* (Cambridge University Press, Cambridge, 2005).
- [29] J. W. M. Bush, The anomalous wake accompanying bubbles rising in a thin gap: A mechanically forced Marangoni flow, *J. Fluid Mech.* **352**, 283 (1997).
- [30] F. Gallaire, P. Meliga, P. Laure, and C. N. Baroud, Marangoni induced force on a drop in a Hele Shaw cell, *Phys. Fluids* **26**, 062105 (2014).

- [31] A. Oberbeck, Ueber stationaere fluessigkeitsbewegungen mit beruecksichtigung der inneren reibung, *J. Reine Angew. Math.* **81**, 62 (1876).
- [32] H. Brenner, Effect of finite boundaries on the stokes resistance of an arbitrary particle, *J. Fluid Mech.* **12**, 35 (1962).
- [33] A. M. J. Davis, Slow viscous flow due to motion of an annular disk; Pressure-driven extrusion through an annular hole in a wall, *J. Fluid Mech.* **231**, 51 (1991).
- [34] J. F. Trahan, R. G. Hussey, and R. P. Roger, The velocity of a circular disk moving edgewise in quasi-steady Stokes flow toward a plane boundary, *Phys. Fluids* **11**, 2463 (1999).
- [35] J. F. Trahan, Stokes drag on a thin circular disk moving edgewise midway between parallel plane boundaries, *J. Fluids Engineering* **128**, 887 (2006).
- [36] L. Landau and B. Levich, *Physicochim. Acta. Physicochim (URSS)* **17**, 42 (1942).
- [37] B. V. Derjaguin, *Doklady Akademii nauk SSSR* **39**, 13 (1943).
- [38] A. Huerre, V. Miralles, and M.-C. Jullien, Bubbles and foams in microfluidics, *Soft Matter* **10**, 6888 (2014).
- [39] I. Cantat, Liquid meniscus friction on a wet plate: Bubbles, lamellae, and foams, *Phys. Fluids* **25**, 031303 (2013).